Journal of Asian Earth Sciences 166 (2018) 223–232

Contents lists available at ScienceDirect

Journal of Asian Earth Sciences

journal homepage: www.elsevier.com/locate/jseaes

Full length article

Holocene climatic evolution at the Chinese Loess Plateau: Testing sensitivity to the global warming-cooling events

Taslima Anwar[a,b], Vadim A. Kravchinsky[b,a,*], Rui Zhang[a,b,c,*], Lioudmila P. Koukhar[b], Lirong Yang[a], Leping Yue[a,c]

[a] State Key Laboratory of Continental Dynamics, Department of Geology, Northwest University, Xi'an 710069, China
[b] Department of Physics, University of Alberta, Edmonton, Alberta T6G 2E1, Canada
[c] State Key Laboratory of Loess and Quaternary Geology, Institute of Earth Environment, Chinese Academy of Sciences, Xi'an 710075, China

ARTICLE INFO

Keywords:
Climate change
Chinese loess-paleosol sequence
Holocene
Magnetic susceptibility
Petromagnetism
Soil

ABSTRACT

A high resolution petromagnetic analysis demonstrates that pedogenic alterations in Holocene loess (sand) sequences from the regions of the Guanzhong Basin and the Mu Us Desert on the Chinese Loess Plateau (CLP) were affected by climatic variations in temperature and precipitation. Three warm-humid intervals (~8.4–3.7, ~2.4–1.2, and ~0.81–0.48 ka), associated with soil formation and relatively high values of petromagnetic parameters, occurred during the Holocene. A substantial paleosol development from ~8.4 to 3.7 ka and higher petromagnetic parameter values indicate a generally strong warm-humid phase in the mid-Holocene which can be attributed to the Holocene climatic optimum. Our study demonstrates that the Holocene climate in the eastern part of the CLP is sensitive to warming and cooling events linked to global changes in temperature and precipitation. A complete Holocene climate record is constructed, correlating well with the other regional climate records along the south-to-north profile on eastern CLP, and suggesting that similar climatic changes occurred in eastern monsoonal China during the Holocene. Results are supported by other climate records in different regions of the world, and imply that the Holocene climatic optimum in the northern hemisphere probably took place at the same time.

1. Introduction

Many paleoclimate studies have underlined climate fluctuations in the Holocene interval in many places (Steig, 1999, Bianchi and McCave, 1999; Wurster and Patterson, 2001; Baker et al., 2001; McDermott et al., 2001 and others). Studies have explored six such fluctuations across the globe with an indication of polar cooling, tropical aridity, and significant atmospheric deviations (Mayewski et al., 2004). Although the development of current human civilization has been nurtured by the Holocene climate, there is quite a limited knowledge of the link between regional and global climate variability during this period. However, this limitation can be addressed through the approach of comprehensive paleoclimate data collecting from different locations of the globe, particularly from climate-sensitive ones. Arid and semi-arid China provides a highly sensitive and broad area for large-scale climatic variations (Thompson et al., 1989; Feng et al., 1993; D'Arrigo et al., 2000; Jacoby et al., 2000).

The Holocene climates and environments of the Chinese arid zone have been investigated for quite a long time (Zhu et al., 1982; Liu, 1985; An et al., 2000; Xiao et al., 2004; Feng et al., 2006; Zhou et al., 2010 and others). Various records and archives including pollen and loess stratigraphy, variations in lake and sea-levels, lacustrine sediments and ice cores with stable isotopes have been studied and correlated to reconstruct climatic variations in the Holocene. Particularly, pollen data, fossil fauna, paleosol, lake level, glacial remains, and archaeological data in China considered the mid-Holocene (ca. 9.4–3.1 ka) to be a climate optimum (Shi et al., 1992; Li, 1996). Based on the analyses of various records of paleoclimatic imprints or proxies, He et al. (2004) suggested that the Holocene climate optimum occurred at 6.5–5.5 ka in eastern China. For each area in China, the Holocene climate had three distinct phases, and the middle Holocene optimum (8–5 ka) occurred in arid to semi-arid areas (Feng et al., 2006). Studying independent proxies including contemporary pollen data, Herzschuh (2006) deduced that the Holocene optimum, characterized by high precipitation, occurred at the different time period in Indian monsoon and East Asian monsoon regions; it occurred during the early Holocene and the mid-Holocene respectively for these regions. In northwest China, multi-proxy analyses indicate that variable dry

* Corresponding authors at: Department of Physics, University of Alberta, Edmonton, Alberta T6G 2E1, Canada.
E-mail addresses: vadim@ualberta.ca (V.A. Kravchinsky), ruizhang@nwu.edu.cn (R. Zhang).

https://doi.org/10.1016/j.jseaes.2018.07.032
Received 2 December 2017; Received in revised form 15 July 2018; Accepted 21 July 2018
Available online 23 July 2018
1367-9120/

climate occurred from 7.8 to 1 ka (Zhao et al., 2010). Zhang et al. (2015) showed, studying the pollen data of eastern Qinghai–Tibetan Plateau, that the climate was wet due to the presence of a strong southwest Asian monsoon during 11–8.7, 8–6, and 5.6–1.7 ka. Prevalence of the highest moisture is evident in arid Central Asia in the mid-Holocene (between 7.5 and 5.5 ka) as constant lake conditions and lower salinities in that time in the region were documented (Mischke et al., 2016). In Horqin dune field, a low density of vegetation coverage occurred between ~11 and ~8 ka associated with a dry climate; whereas vegetation coverage was high between ~8 and ~3.2 as well as ~2.8 and ~2.6 related to a warm and humid climate (Mu et al., 2016). As there has been a discourse among the Quaternary scientists on climatic variations in China in different intervals of the Holocene, it requires more clarification and a better understanding of this climate change through the detailed records from various sources.

Selecting proper proxies and developing reliable chronologies is the key to reconstructing variations in climate and environment during the Holocene. In arid and semi-arid regions, loess-paleosol sequences react to climatic variations, indicating that these areas are suitable for investigating the evolutions of paleoclimate and paleoenvironment (Rutter, 1992; Ding et al., 1993; Maher, 2011). These sequences can be instrumental to reconstruct climatic history of neighboring regions of the Loess Plateau through the last glacial cycles (e.g., Vandenberghe et al., 1997; Sun et al., 1999; Lu et al., 1999, 2000). It is clear that more complex Holocene loess-paleosol sequences exist, and these are attributable to fluctuations in monsoonal climate (Zhou and An, 1994; Huang et al., 2000). Enhanced magnetic properties, consequential of interglacial pedogenesis, are now a fact acknowledged by the rock-magnetic community (Evans and Heller, 2003). During interstades, climate is warmer and, generally, wetter due to the strengthening of summer monsoon circulation (Porter, 2001). Such process leads to enhanced pedogenesis and production of low-coercivity magnetic minerals (Deng et al., 2001; Liu et al., 2004; Li et al., 2015). At the same time, inter-stadial soils are typically less developed because of continuous dust influx and dilution (Porter, 2001). Deng et al. (2001), Maher et al. (2003) and Kravchinsky et al. (2013) demonstrated that the Holocene soil-loess formation also follows that model where rock-magnetic parameters are enhanced in soils. For all these, the loess-paleosol records with reliable chronology are critical to understanding the overall pattern of climate variations in monsoonal China during the Holocene.

The analysis of petromagnetic properties of loess-paleosol deposits is instrumental in interpreting paleoclimatic conditions during the time of their accumulation (Evans and Heller, 2003). In this study, these properties, along with sedimentary grain size, are analyzed to investigate the Holocene climatic variations focusing on the loess-paleosol profiles within the Guanzhong Basin and the Mu Us Desert regions which are in East Asian monsoonal zone. The Guanzhong Basin is located at the southern edge of the Loess Plateau whereas the Mu Us Desert is situated at the northern part of the Plateau. Our study aims to reconstruct regional climate and environmental changes in the Holocene recorded by the Chinese Loess; to explore the influence of temperature, precipitation, and wind strength on regional climate changes; to understand the responses of regional Holocene climate along the south-to-north eastern Chinese Loess Plateau; and to investigate whether regional Holocene climate changes in China share common characteristics to globally averaged Holocene climate change or have distinct characteristics.

2. The study area

In this study, five aeolian sections located in two different areas, Yaozhou in the Guanzhong Basin and Jinjie in the Mu Us Desert, were sampled. Yaozhou (34°53′N, 108°58′E) is situated about 60–70 km east of Xi'an city (YZ in Fig. 1). At middle zone of the Yellow River valley, the Guanzhong Basin is located in the southern part of the Loess Plateau

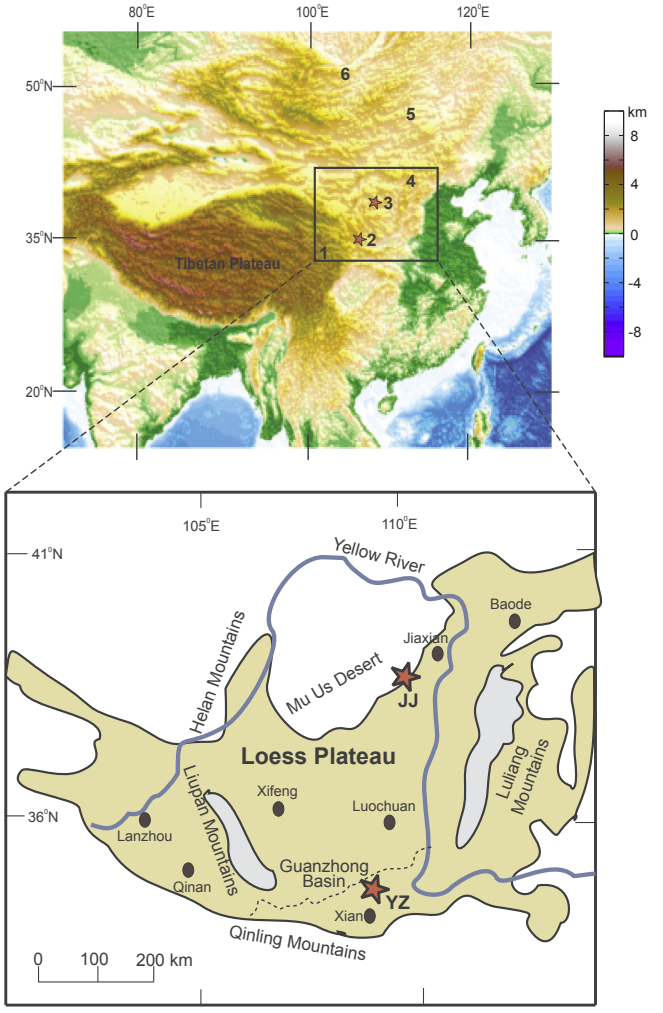

Fig. 1. Top: satellite image map showing the location of the studied areas (red star) and the other sites discussed in the text: 1 – Hongyuan peatland (32°47′N, 102°31′E); 2 – Yaozhou (34°53′N, 108°58′E); 3 – Jinjie (38°74′N, 110°9′E); 4 – Daihai Lake (40°29′N, 112°33′E); 5 – Hulun Lake (48°31′N, 112°00′E); 6 – Lake Baikal (51°58′N, 104°85′E). Bottom: geographic location of Yaozhou (YZ) and Jinjie (JJ) studied areas in the Chinese Loess Plateau. (For interpretation of the references to color in this figure legend, the reader is referred to the web version of this article.)

to the north of the Qinling Mountains (Fig. 1). Land surface in the Guanzhong Basin has been quite settled because of less erosion, and eventually, it has made the aeolian dust deposits and soil surface well-preserved during the entire Holocene period (Huang et al., 2000). In the Guanzhong Basin, a few Holocene loess-paleosol studies have been published; they examined changes in vegetation (Li et al., 2003) and in climate at the Yaoxian locality (Zhao et al., 2007), as well as cultural effect at the Qingquicun locality (Huang et al., 2000). Present mean annual temperature is 13 °C while mean annual rainfall is around 554 mm, and these are associated with a semi-humid climate that displays significant seasonal variations in temperature and precipitation which become intense in summer (Zhao et al., 2007). Three sections were investigated from this locality within two excavated pits: the first section (YZ1), the second one at 100 m further south (YZ2), and the third one at 300 m west from the first one (YZ3). YZ2 is at the same pit of YZ1, whereas YZ3 is at a different pit. The sequence of 5 m YZ1, 3.3 m YZ2 and 4 m YZ3 are composed of three paleosol units of Holocene age (S_0S_1, S_0S_2, and S_0S_3), interbedded with two layers of loess. The stratigraphic unit was identified through an examination of color, texture, and structure of the sediment. However, the buried soils in

these sections cannot be identified very well visually in the field but can be confirmed through the magnetic measurements.

Jinjie (38°44′N, 110°9′E) is located at the southeastern margin of the Mu Us Desert (JJ in Fig. 1). The Mu Us Desert, being situated at northern-central China and having sand dunes, belongs to the peripheral region of East Asian monsoon. Currently, almost two-thirds of this desert is covered by sand dunes (Sun, 2000). The ecosystem, in the semi-arid Mu Us Desert, exhibits a high sensitivity towards climate change since external climatic forces can easily affect the vegetation, soil, and aeolian sand (Sun et al., 2006). The local mean annual temperature in the Mu Us Desert, currently, varies from 6 to 9 °C, and the mean annual rainfall is 200–400 mm (Ma et al., 2011). 70% of the rainfall concentrates from July to September, with a warm and humid summer as well as autumn. In winter, it is cold and dry with the prevailing cold northwestern winds. Two sections from Jinjie area, JJ1 (along the road) and JJ3 (along the road and about 1 km southeast from JJ1), were studied. 7 m deep JJ1 and 8 m deep JJ3 aeolian sequences contain three distinctive dark brown sandy loam soil layers (S_0S_1, S_0S_2, and S_0S_3) separated by sand beds. The stratigraphic subdivision was made by field observations of color, texture, and structure of the sediment. The correlation between two sections was done in the field; three soil horizons could be traced visually between both sections on the slope of the excavated road wall. For JJ3 section, there is a mixture of sand and soils in between two soil layers. All of these sections are situated above the Malan loess (L1).

Yaozhou loess-paleosol and Jinjie sand-paleosol sequences are both dated using optically stimulated luminescence (OSL) dating technique (Zhao et al., 2007; Ma et al., 2011). In Yaozhou, the boundary between the lowest paleosol (S_0S_3) and the Malan Loess was OSL dated 8.44 ± 0.59 ka (Zhao et al., 2007). At Jinjie, the lowest paleosol (S_0S_3) was bracketed by two OSL dates – 7.07 ± 0.42 ka at the bottom and 3.91 ± 0.18 ka at the top (Ma et al., 2011). Ages of each soil section are assigned based on the OSL dating of Zhao et al. (2007) for Yaozhou area and Ma et al. (2011) for Jinjie area. Our sampling was performed jointly with J. Ma and her co-authors (Ma et al., 2011) in order to warrant correct matching between depths and ages; Li. Y. and Le. Y. are the co-authors of the current study.

3. Methods

3.1. Sampling

A total of 573 non-oriented bulk samples were collected from the 5 sections (YZ1: 100, YZ2: 80, YZ3: 85, JJ1: 150 and JJ3: 158 samples) for petromagnetic and sedimentary grain size analyses. Samples were taken continuously at 5 cm intervals (2.5 cm intervals only for the thin soils) from all sections. Sampling was started from the top that contains present-day soil i.e. the cultivated layer.

3.2. Thermomagnetic and hysteresis data

Temperature-dependent magnetic susceptibility was measured on several (4–6) samples from each section to investigate magnetic mineralogy. The measurement was performed using a Bartington susceptibility meter in the Laboratory of Paleomagnetism and Petromagnetism of the Department of Physics at the University of

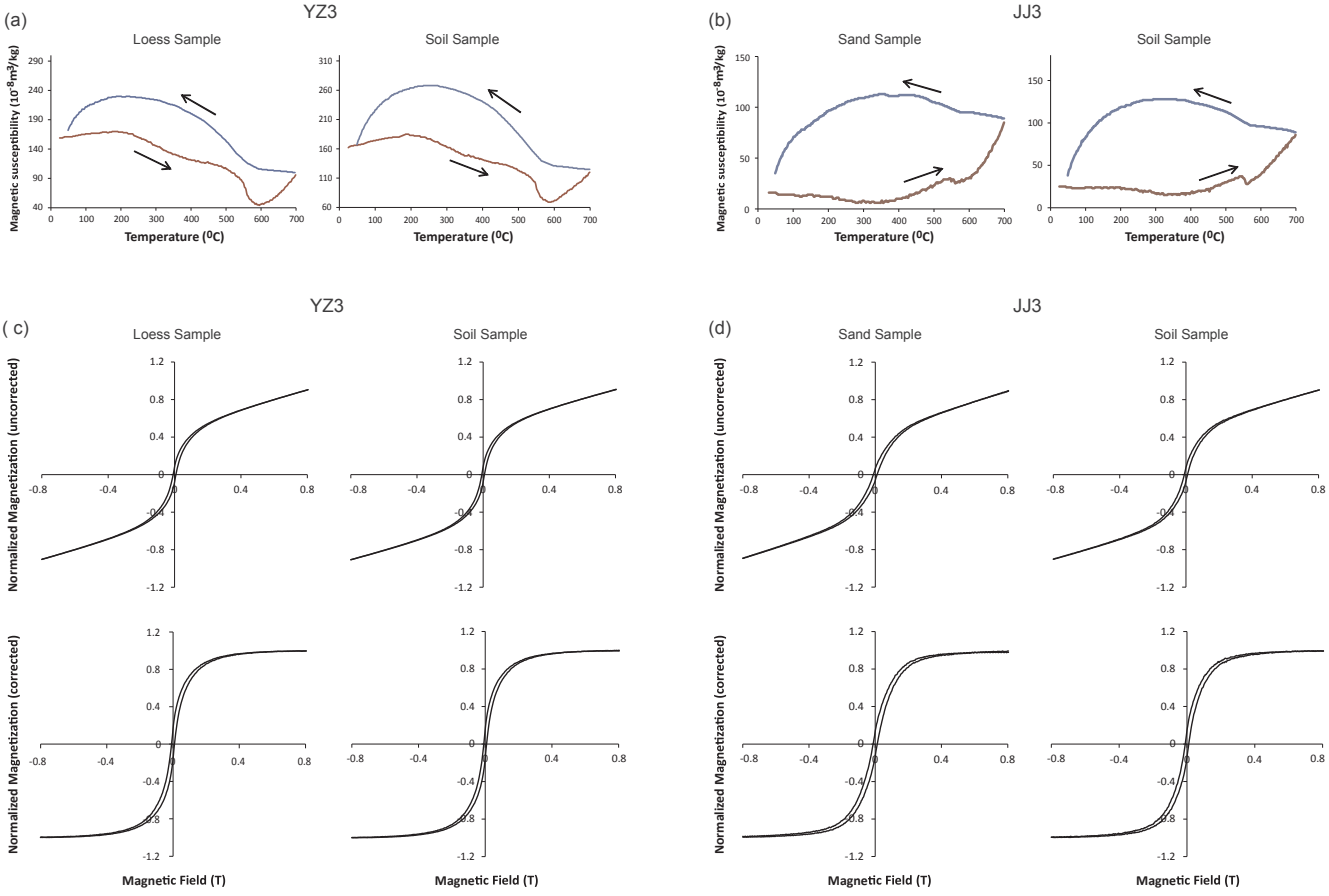

Fig. 2. Top: examples curves of temperature dependent magnetic susceptibility. Arrows represent heating (red line) and cooling (blue line) directions. (a) Samples from YZ3 section (loess; sample 205 and soil; sample 150), (b) samples from JJ3 section (sand; sample 275 and soil; sample 175). Bottom: representative uncorrected and corrected hysteresis loops. (c) samples from YZ3 section (loess; sample 50 and soil; sample 250), (d) samples from JJ3 section (sand; sample 30 and soil; sample 540). (For interpretation of the references to color in this figure legend, the reader is referred to the web version of this article.)

Alberta. The sample was heated up to 700 °C and then allowed to cool back to room temperature in the air. During heating and cooling, magnetic susceptibility measurement of the sample was taken at every 2 °C. The magnetic grain size of the samples (10 samples from each section) was investigated by hysteresis measurements at room temperature with a maximum field of ± 1 T using a VFTB in the Environmental Magnetism Laboratory, Geophysics Institute in Beijing, China. Saturation magnetization (Ms), remanent saturation magnetization (Mrs), coercive force (Hc), and the coercivity of remanence (Hcr) values were evaluated from hysteresis loops.

3.3. Petromagnetic parameters

A number of petromagnetic parameters such as low and high frequency magnetic susceptibility, anhysteric remanent magnetization (ARM), saturation isothermal remanent magnetization (SIRM), and back field isothermal remanent magnetization (bIRM) were measured to identify variations in concentration, grain size and mineralogy of magnetic material in the samples. These were conducted in the Laboratory of Paleomagnetism and Petromagnetism of the University of Alberta. These parameters (low field mass specific magnetic susceptibility χ_{lf} and SIRM) and the ratios derived from them (frequency dependence of magnetic susceptibility FD and normalized to the steady field anhysteric remanent magnetization χ_{ARM}) were used to interpret paleoclimatic conditions during deposition of the studied sections.

In the laboratory, 8 cm^3 plastic non-magnetic boxes were used to host the sediments for petromagnetic measurements. Low-frequency (0.465 kHz) and high-frequency (4.65 kHz) magnetic susceptibility of each sample were measured using a Bartington Instruments MS2B dual frequency meter. To reduce the level of considerably high noise from the Bartington instrument, special precaution was taken during measurements. Each sample was measured three times in different positions, and the average magnetic susceptibility value was calculated for both low and high frequency measurements. All the values were checked before getting the average and found consistent without high errors. Air measurements were taken in between two samples' measurement each time to monitor and eliminate the instrumental drift. FD value was calculated for each sample using its averaged low and high frequency magnetic susceptibility values. ARM was acquired in a peak AF field of 100 mT and a steady DC field of 0.1 mT by a 2G cryogenic magnetometer demagnetizer. This ARM was normalized to the steady field to yield χ_{ARM}. SIRM was acquired in a field of 0.6 T through a 2G IRM stand-along electromagnet. bIRM was induced to the samples by using a reversed field of 0.3 T and the acquired remanences were measured on the cryogenic magnetometer. Parameters (χ_{ARM}/χ_{lf} and $\chi_{ARM}/SIRM$) were also evaluated for each sample.

3.4. Sedimentary grain size

Sedimentary grain size analysis was performed in order to determine relative wind strengths during loess deposition of the studied sections. Sedimentary grain size was measured on a Mastersizer 2000 laser particle analyzer at Northwest University in Xi'an, China. The grain size samples were subjected to standard chemical pretreatment. To eliminate organic material, samples of 0.3–0.4 g were fully dissolved in 10 ml of 10% boiling hydrogen peroxide (H_2O_2) solution in a 200 ml beaker. Carbonates were also removed by boiling with 10 ml of 10% hydrochloric acid (HCl). Distilled water was added during the chemical treatment to avoid drying of the solution. After standing overnight, clear water was decanted from the sample. Through a combination of an addition of 10 ml of 10% sodium hexametaphosphate [$(NaPO_3)_6$] solution and an oscillation for around 10 min ultrasonically, the sediment particles were dispersed.

4. Results

4.1. Thermomagnetic and hysteresis

Typical examples of temperature dependent magnetic susceptibility curves in the air and hysteresis loops are presented in Fig. 2. The magnetic susceptibility shows a decrease in signal and reaches minimum value before 590 °C, indicating the presence of magnetite (Butler, 1992) (Fig. 2). Magnetite is a typical climate proxy in the Chinese classical and Holocene loess (Deng et al., 2000). Further, we observed that the magnetic susceptibility values start to increase above 590 °C and the cooling curves are not reversible, suggesting that new magnetic minerals are produced by an oxidation in the sample. The color of the samples changed to dark brown indicating production of some hematite at least at the sample surface additionally to a high magnetic susceptibility value magnetic mineral. Such thermomagnetic behavior is not described for the Chinese Holocene loess samples heated in the air; which are usually heated and cooled in argon atmosphere (Deng et al., 2000). Transformation of magnetite to hematite is reported through a formation of maghemite (Nasrazadani and Raman, 1993), which may be a possible explanation of the change of color during the heating above 590 °C. The increase in susceptibility could be due to a transformation from iron-containing silicates and clays to magnetite during the heating (Deng et al., 2000). For the present-day loess, the presence of some organic matter and adsorbed iron may create locally reducing conditions and provide irons needed for new magnetite when the heating was done in argon (Hanesch et al., 2006).

The shape of hysteresis loops indicates samples contain pseudo-single domain (PSD) particles (Fig. 2). The slopes of the high field segments of hysteresis loops prior to high field slope correction are positive for all samples demonstrating that paramagnetic fraction is presented in the bulk material. The remanence ratio (Mrs/Ms) versus coercivity ratio (Hcr/Hc) is shown on a Day plot (Dunlop, 2002) in Fig. 3. The Day plot implies that mean magnetic grain size of samples mainly clusters within the pseudo-single domain (PSD) region (Fig. 3). However, hysteresis parameter distribution on a Day diagram for the samples of JJ1 and JJ3 sections is more spread out compared to that of YZ3 section. JJ sections are sandy and are situated closer to the source of the parental material in the Mu Us Desert; therefore, it is expected that grain size variations of JJ sections are larger than that of YZ loess

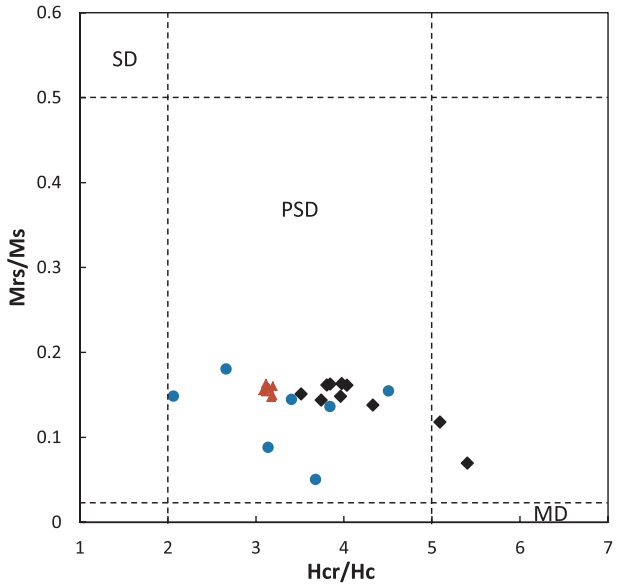

Fig. 3. Day plot of the hysteresis parameters (based on Dunlop, 2002) for YZ3 (triangles), JJ1 (diamonds), and JJ3 (circles) sections. SD – single domain; PSD – pseudo-single domain; and MD – multidomain.

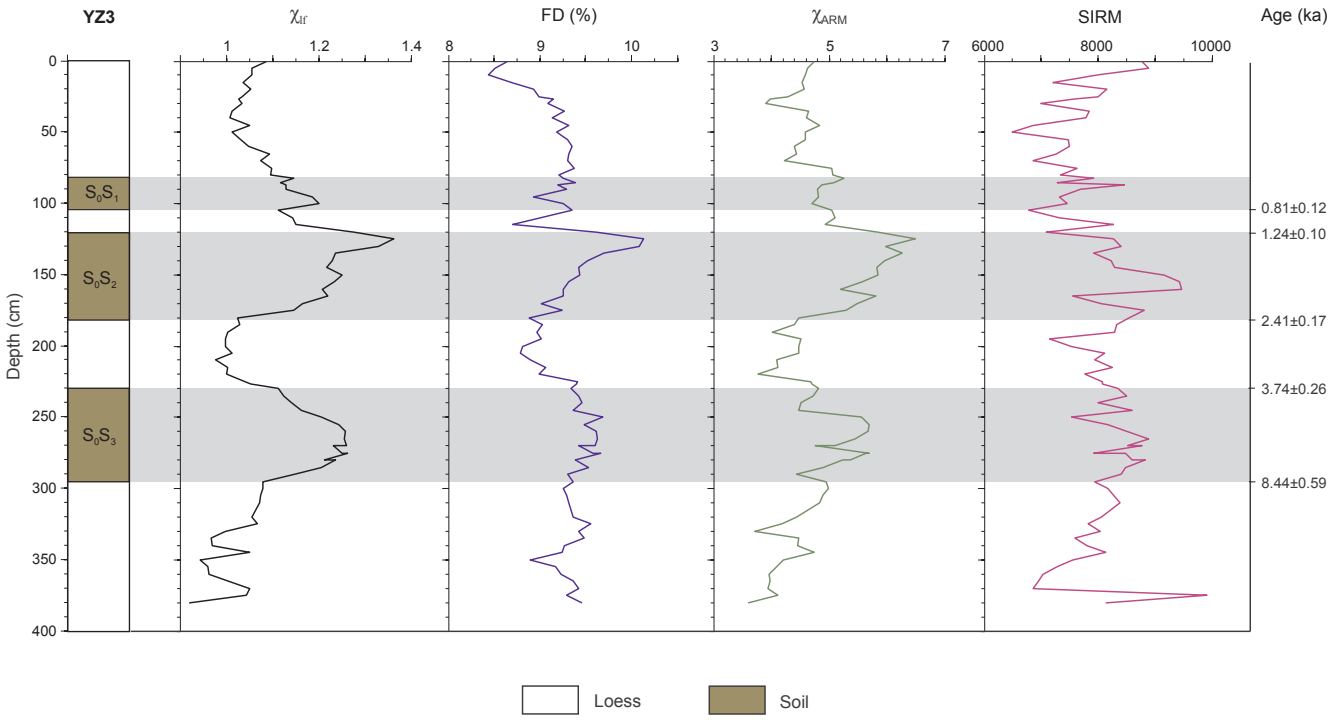

Fig. 4. Stratigraphy and magnetic concentration parameters of YZ3 section. χ_{lf} – low frequency magnetic susceptibility ($10^{-6}\,m^3\,kg^{-1}$); FD (%) – frequency dependence parameter; χ_{ARM} – anhysteric remanent magnetization ($10^{-6}\,m^3\,kg^{-1}$); and SIRM– saturation isothermal remanent magnetization ($10^{-6}\,A\,m^2\,kg^{-1}$). Horizontal grey bars denote soil horizons, interpreted as relatively warm-wet intervals.

sections.

4.2. Petromagnetic parameters

The measured parameters of five sections (YZ1, YZ2, YZ3, JJ1, and JJ3) have been plotted against the depth of the sections in Figs. 4 and 5 and Supplementary Figs. S1–S3. Magnetic susceptibility has become a standard proxy to investigate Quaternary climate change in loess-paleosol sequences on the Chinese Loess Plateau (Heller and Liu, 1984; Balsam et al., 2004). The magnetic susceptibility record demonstrates variations of the pedogenesis intensity caused by precipitation changes related to summer monsoon climatic fluctuations (An et al., 1991; An and Xiao, 1990; Maher and Thompson, 1995; Maher, 2011). χ_{lf} measures the magnetic response caused by remanence-carrying and non-remanence-carrying mineral components present in the samples

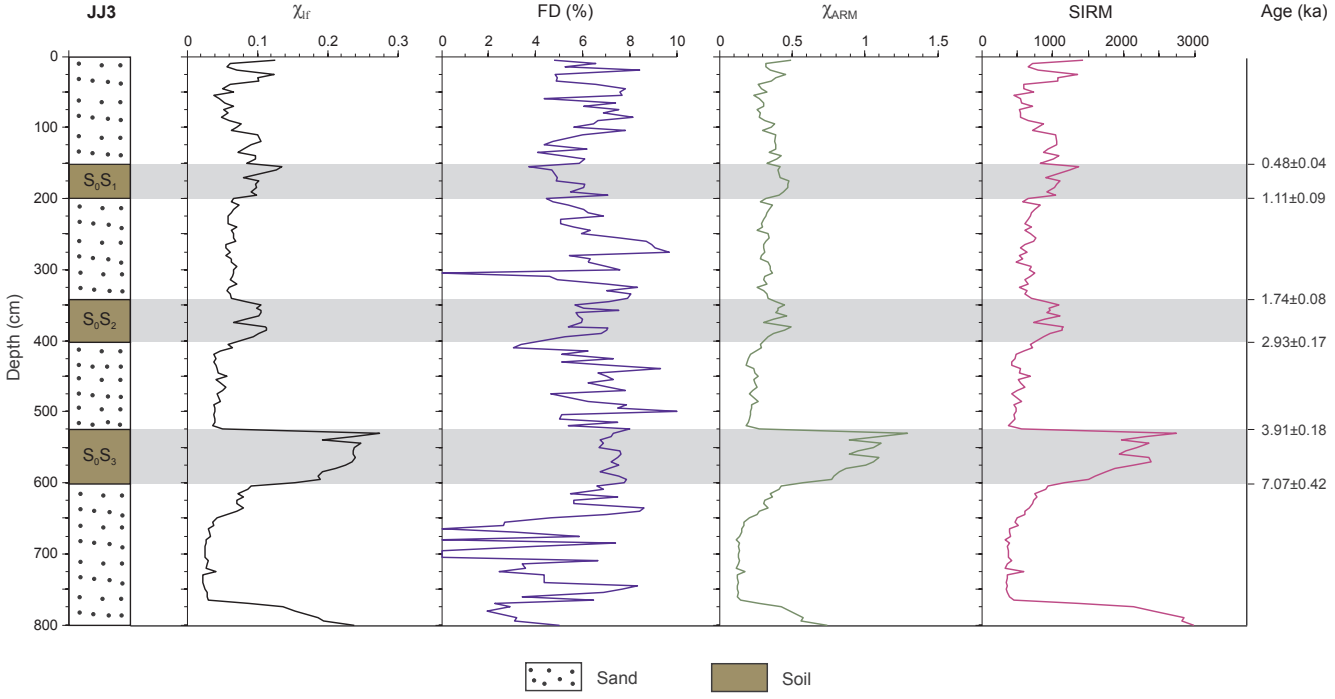

Fig. 5. Stratigraphy and magnetic concentration parameters of JJ3 section. Same abbreviations as in Fig. 4.

(Robinson, 1986; Thompson and Oldfield, 1986; Evans and Heller, 2003). χ_{lf} values (average $0.13 \times 10^{-6}\,m^3\,kg^{-1}$) for Jinjie area (JJ1 and JJ3 sections) are relatively lower than those (average $1.05 \times 10^{-6}\,m^3\,kg^{-1}$) of Yaozhou area (YZ1, YZ2, and YZ3 sections), suggesting that the latter area probably has a higher concentration of magnetic particles. However, Yaozhou area has systematically higher FD parameter indicating that a greater proportion of superparamagnetic grains can increase magnetic susceptibility without increasing the actual concentration of magnetic particles. The parent material is different for Yaozhou and Jinjie localities; it is loess and sand respectively. Although the pedogenic degree varies for five sections may be due to parent materials, sedimentation mechanism, and redeposition, the loess/sand and paleosol layers are all clearly identifiable in the χ_{lf} profiles from all sections (Figs. 4 and 5 and Figs. S1–S3). In this study, susceptibility curves (χ_{lf}) of all the sections show that the soils have a higher susceptibility compared to the loess/sand beds (Figs. 4 and 5 and Figs. S1–S3), indicating warm-wet climate conditions during the formation of these accretionary soils. On the other hand, lower χ_{lf} values in the loess/sand layers exhibit a cool-dry climate and intensified aeolian dust deposition as well as weak pedogenic processes during loess deposition. The upper layer of the soils (S_0S_1), formed thinner in a shorter period, shows weak χ_{lf} values almost as same as the values of adjacent aeolian loess/sand, whereas the lower layers of soils represent stronger signals for the sections YZ2, YZ3, JJ1, and JJ3 (Figs. 4 and 5 and Figs. S2 and S3). For YZ1 section, S_0S_1 shows a high peak with disturbance due to the close proximity of S_0S_1 to modern soil or cultivated layer documented in the field (Fig. S1).

Supplementary data associated with this article can be found, in the online version, at https://doi.org/10.1016/j.jseaes.2018.07.032.

The FD parameter appears to be higher in soil horizons compared to the loess as it is related to the distribution of ferromagnetic minerals, commonly superparamagnetic magnetite produced during soil formation (Thompson and Oldfield, 1986; Evans and Heller, 2003). Most of the soil horizons exhibit higher FD values (ranging around 8–10%) compared to their respective parent loess (YZ) or sand (JJ) horizons, and these are in agreement with the χ_{lf} values (Fig. 4 and Figs. S1–S3). These higher FD values of studied soil horizons confirm continuous production of superparamagnetic particles during the pedogenesis in warmer and/or wetter interval. However, for JJ3 section, the FD parameter does not show variations to corresponding sands and soils (Fig. 5), probably due to sandiness of the soils for this section.

χ_{ARM} and SIRM indicate variations in magnetic mineral concentration, and values get higher with increasing concentration of minerals, excluding superparamagnetic particles, having a high magnetization such as magnetite (Thompson and Oldfield, 1986; Yu and Oldfield, 1989; King and Channell, 1991; Evans and Heller, 2003). Figs. 4 and 5 and Figs. S1–S3 indicate that the paleosol horizons have higher χ_{ARM} and SIRM values compared to the loess/sand horizons. The higher χ_{ARM} and SIRM values represent a higher concentration of magnetic particles within the soil layers, and indicate warmer-wetter conditions and active pedogenic processes during the time of soil formation. Whereas lower values, found in the loess/sand layers, indicate cooler-drier conditions and weak pedogenic intensity during the periods of intensified dust deposition. For all the sections, χ_{ARM} and SIRM curves indicate the presence of χ_{lf} and FD peaks, corresponding to the soil horizons (Figs. 4 and 5 and Figs. S1–S3).

4.3. Sedimentary grain size

The grain size variations of loess deposits have commonly been used to monitor past wind intensity changes (Pye and Zhou, 1989; Rea, 1994). Stronger winds are associated with more dust storms, coarser particle size, and larger dust input to the Loess Plateau (Ding et al., 1994). The average median grain size values are larger for Jinjie area (~220 μm) than Yaozhou area (~13.9 μm), representing that the grain size records of the Holocene loess/sand deposits decrease from north to south over the Chinese Loess Plateau. The grain size of the last glacial loess deposits also displays an overall southward decrease (Yang and Ding, 2004) as the loess was created primarily in the sandy Gobi deserts in northwestern China and was carried away by near-surface northwesterly wind (Liu, 1985; An et al., 1991). However, recent studies suggested that Yellow River brought significant amounts of sediment which is the main source of aeolian supply to the Chinese Loess Plateau (Nie et al., 2015; Licht et al., 2016). Median grain size of the studied sections does not demonstrate general characteristic of the smaller values for the soil horizons well (example Figs. S4 and S5), indicating that the wind intensity did not vary much for these areas during the Holocene.

The ratios χ_{ARM}/χ_{lf} and $\chi_{ARM}/SIRM$ indicate variations in magnetic grain size and the values decrease with increasing magnetic grain size (Thompson and Oldfield, 1986; King et al., 1982; Maher, 1988; Evans and Heller, 2003) taking in account specific assumptions about the presence of only soft ferromagnetic contribution and no changes to SD and MD proportions. For the ratio χ_{ARM}/χ_{lf}, the value also decreases with an increase of the relative amount of superparamagnetic particles. For all the sections, magnetic grain size (χ_{ARM}/χ_{lf} and $\chi_{ARM}/SIRM$) varies in the same manner as the sedimentary grain size does. Both the ratios reflect a little variability for loess/sand and soil horizons indicating smaller relative changes in magnetic grain sizes. Therefore, grain size analysis of the studied sections did not provide any interpretable result.

4.4. Variations in the Holocene climate

Three soil layers (S_0S_1, S_0S_2, and S_0S_3) are identified for all the sections by higher magnetic concentration parameters (χ_{lf}, χ_{ARM}, SIRM) and FD parameter. Therefore, χ_{lf}, FD, χ_{ARM}, and SIRM are higher for soil and lower for loess/sand horizons, indicating warmer and colder assemblage respectively. The sedimentary and magnetic grain size variations do not correspond to the soil intervals entirely. Furthermore, magnetic concentration parameters and FD parameter show a larger variation for the loess/sand and soil layers compared to sedimentary and magnetic grain sizes for these layers. It demonstrates that humidity fluctuation, which is related to vegetation and soil formation, was stronger than wind intensity variation for the studied sections during the Holocene.

Petromagnetic analysis of five sections in Yaozhou and Jinjie areas shows clear changes in regional climate and provides paleoenvironmental information over the Holocene. Changes of parameters with soil formation in five studied sections, at Yaozhou (Jinjie), suggest three distinct warm-humid time periods during the Holocene: the oldest warmer interval was between 8.4 and 3.7 ka (7.0–3.9 ka), the middle one occurred between 2.4 and 1.2 ka (2.9–1.7 ka), and the youngest started at 0.81 ka (1.1 ka) (Figs. 4 and 5 and Figs. S1–S3). Furthermore, based on the data, two cold-dry intervals associated with loess/sand deposition can be considered at Yaozhou (Jinjie): 3.7–2.4 ka (3.9–2.9 ka) and 1.2–0.81 ka (1.7–1.1 ka). However, in these areas, the onset and termination of warming-cooling intervals during the Holocene were almost similar with a slight difference. A subsequent warm-humid phase took place between ~8.4 ka and ~3.7 ka indicated by the development of strong soil (S_0S_3) in all five sections. Combined with high values of all petromagnetic parameters in the studied regions (Figs. 4 and 5 and Figs. S1–S3), this period is attributed to the Holocene optimum, a warm period (generally warmer than today) in the middle of the Holocene. Soil S_0S_3 formation terminated around ~3.7 ka, suggesting a cold-arid period. This resulted in an active period for the loess/sand during ~3.7–2.4 ka. The soil S_0S_2 developed between ~2.4 and ~1.2 ka, and at that time, the values of petromagnetic parameters indicate a warm-humid period in this region (Figs. 4 and 5 and Figs. S1–S3). The climate became colder and drier between ~1.2 and ~0.81 ka as the loess/sand was deposited, illustrated by low values of petromagnetic parameters. Soil S_0S_1 formed in an interval of

~0.81–0.48 ka (Figs. 4 and 5 and Figs. S1–S3), suggesting a warm-humid period.

5. Discussion

5.1. Comparison of regional paleoclimatic records

Changes in climate in the studied sections can be compared with other reported paleoclimatic records from the neighboring monsoonal region of semi-arid China. In this study, we used tree pollen records (Zhou et al., 2010; Xiao et al., 2004; Wen et al., 2010) from peatlands or lakes, located along the south-to-north regional transect on the eastern Loess Plateau, to make a comparison with our results. In order to compare, low frequency χ_{lf} of YZ3 section from Yaozhou and JJ3 section from Jinjie have been selected as representative sections since the soil intervals were identified in these sections better. Various factors such as slope orientation towards the sun and/or wind, slope inclination, amount of vegetation, quality of preservation of original material and amount of excavation during road construction or quarry excavation may affect sections from the same site differently, even if the sections are just a few meters apart. Common practice is to choose the most representative section or to create a stack from all sections. For this reason, we need to consider a number of sections from each site to investigate exact climatic variations and to determine which section can be chosen as representative. Based on our analysis above, we chose YZ3 and JJ3 as representative sections as they recorded climatic changes in the best manner.

The sites we compare with along the south-north transect include the Hongyuan peatland (Zhou et al., 2010), the Yaozhou (YZ3), the Jinjie (JJ3), the Daihai Lake (Xiao et al., 2004), and the Hulun Lake (Wen et al., 2010) (Figs. 1 and 6). Summer temperature and precipitation are two dominant climatic factors controlling soil formation as well as pollen assemblages (Shen et al., 2006). Thus, high magnetic parameters and high tree pollen should reflect warm-wet climates. Three warmer intervals of the studied region visually correlate well with the higher pollen data (Fig. 6).

Pollen records from the Hongyuan peatland (Zhou et al., 2010), the Daihai Lake (Xiao et al., 2004), and the Hulun Lake (Wen et al., 2010) show peak tree pollen abundance in the mid-Holocene between ~8.4 and ~3.7 ka (Fig. 6), suggesting a warmer-wetter climate. There is an agreement in the mid-Holocene maximum or climate optimum as documented in our studied sections and other sites (Fig. 6). In the Lake Daihai which is situated at the northeast from the Mu Us Desert, high and stable lake level also occurred at ~8–3 ka (Sun et al., 2009). An ancient wetland existed continuously from ~7.8 to 4 ka at valleys, southeast of the Lanzhou, which is located further west from the Yaozhou (An et al., 2005). A humid mid-Holocene corresponds well with a more recent reconstruction of monsoonal precipitation through various imprints from the Chinese Loess Plateau (Lu et al., 2013). Zhao and Yu (2012) studied most of the sites of the temporary zone, located between the forest and temperate steppe vegetation in northeastern China, and confirmed the presence of the wettest climate occurred between ~8 and ~4 ka. High level of the Lake Huangqihai during 8–4 ka (Shen, 2013), situated in monsoonal region, indicates a strong East Asian summer monsoon happened in the mid-Holocene. In the Horqin dune field, a greater density of vegetation coverage occurred between ~8 and ~3.2 ka, suggesting a warm and humid climate (Mu et al., 2016). Even though the termination of the warm-humid Holocene optimum slightly vary in different sections, this is expected due to the age model imperfections and assumptions of the close to constant sedimentation rate, the inconsistencies of various dating methods or irregularity of the Holocene optimum (e.g., An et al., 2000; He et al., 2004).

From ~3.7 to ~2.4 ka, the decreasing susceptibility of the studied sections suggests a drying and cooling climate trend that correlates with the tree pollen data (Fig. 6). The pollen sequence collected from the Taishizhuang peat site, located at the southeastern edge of the Mongolian Plateau, confirms a significant climatic variation taken place at around ~3.4 ka, and during that time, the tree component almost disappeared entirely (Jin and Liu, 2002; Tarasov et al., 2006). Both in

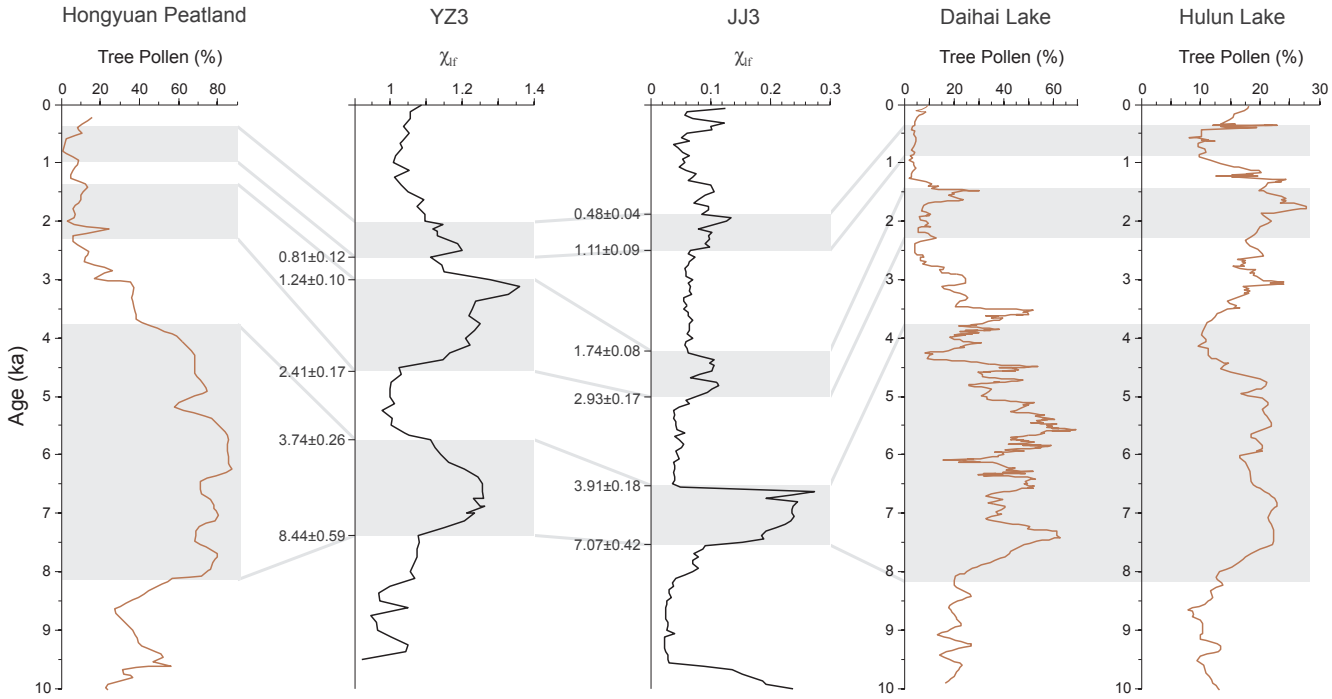

Fig. 6. Comparison of Holocene paleoclimate records in China (from south to north): total tree pollen percentage at Hongyuan peatland (Zhou et al., 2010); χ_{lf} – low frequency magnetic susceptibility (10^{-6} m^3 kg^{-1}) for YZ3 section (this study); χ_{lf} (10^{-6} m^3 kg^{-1}) for JJ3 section (this study); total tree pollen percentage at Daihai Lake (Xiao et al., 2004); and total tree pollen percentage at Hulun Lake (Wen et al., 2010). Locations of these areas are shown in Fig. 1. Grey horizontal bars represent the warm-wet climatic intervals based on the record of this study.

south-central and southeastern Inner Mongolia region, a major cultural shift occurred at ~3.5 ka (Liu and Feng, 2012). After ~3.7 ka, aeolian sand transportation took place more frequently and East Asian summer monsoon strength decayed significantly, as perceived from the higher probability density values (Wang et al., 2014). A drying and cooling climatic shift was also found in two cave speleothem sequences in southern China from the Linhua Cave at ~3.3–3.0 ka (Cosford et al., 2008) and from the Heshang Cave at ~3.6–3.1 ka (Hu et al., 2008).

For the interval of ~2.4–1.2 ka, the magnetic climate data of this study coincides well with the tree pollen data of the Hongyuan peatland (Zhou et al., 2010), the Daihai Lake (Xiao et al., 2004), and the Hulun Lake (Wen et al., 2010) (Fig. 6). This period can be confirmed by moist grassland at the Guanzhong Basin (Li et al., 2003). Furthermore, in Fig. 6, the correlation analysis of magnetic susceptibility and tree pollen data shows good agreement for the cold-dry interval of ~1.2–0.81 ka. Although the warmer interval of ~0.81–0.48 ka, recorded by the magnetic proxies in this study, does not correlate well with the tree pollen data of the Hongyuan peatland (Zhou et al., 2010) and the Hulun Lake (Wen et al., 2010), it shows a good agreement with the tree pollen data of the Daihai Lake (Xiao et al., 2004) (Fig. 6) suggesting that the pollen record in the area does not always register minor variations of climate. Our results are in broad agreement with pollen records and demonstrate that same important climatic variation occurred along the south-to-north eastern Chinese Loess Plateau during the Holocene.

5.2. Comparison of global paleoclimatic records

Our results of Holocene climate changes in China correspond soundly to the global records. We compare our low frequency χ_{lf} records of YZ3 and JJ3 sections with the Lake Baikal $\delta^{18}O$ values from diatom silica (Mackay et al., 2011), temperature variations in the northern hemisphere (McMichael, 2012), and Drift Ice Indices Stack from the North Atlantic (Bond et al., 2001) (Fig. 7). Temperature variations in the northern hemisphere during the Holocene have been reconstructed through an average of various published data (McMichael, 2012). The studied three major episodes correspond visually to the other global records (Fig. 7).

For ~8.4–3.7 ka, our data show high susceptibility and indicate the warm-humid period for the whole interval. Whereas, $\delta^{18}O$ values of the Lake Baikal (Mackay et al., 2011), temperature variations in the northern hemisphere (McMichael, 2012), and Drift Ice Indices Stack from the North Atlantic (Bond et al., 2001) show two peaks during that interval (Fig. 7). The Lake Baikal record sampling resolution is quite low, but it also registers the cooling interval between ~5 and 6 ka very well. There exists no clear indication of such cooling interval in the studied sections, implying that this short-term interval was not registered in the Chinese loess. Nevertheless, the whole interval of ~8.4–3.7 ka in China can be considered a warm and humid period. The period between ~7 and 4.2 ka BP was demonstrated as high summer temperature in the mid and high latitude areas of the northern hemisphere (Klimenko et al., 1996; Alverson et al., 2003). Furthermore, an extensive paleosol, developed on the eastern belt of the Badain Jaran Desert, indicates a climate optimum in the mid Holocene (Yang et al., 2011). Therefore, the interval of ~8.4–3.7 ka can be considered a globally registered Holocene optimum period.

A cool and dry climate from ~3.7 to ~2.4 ka caused the lowest χ_{lf} and well-preserved loess/sand in the studied area, indicated also by other global data (Fig. 7). A cold and arid period from ~3.5 to ~2.5 ka in the northern hemisphere was determined by Mayewski et al. (2004), and this interval is almost the same arid period as found in this study. In the northern hemisphere, 3.5–2.5 ka shows rapid climate change intervals including the North Atlantic ice-rafting events (Bond et al., 1997) as well as strengthened westerlies over the North Atlantic and Siberia (Meeker and Mayewski, 2002). The interval at 3.5–2.5 ka also presents a strong aridity in regions like East Africa, Amazon Basin, Ecuador, and Caribbean/Bermuda region (Haug et al., 2001). Wanner

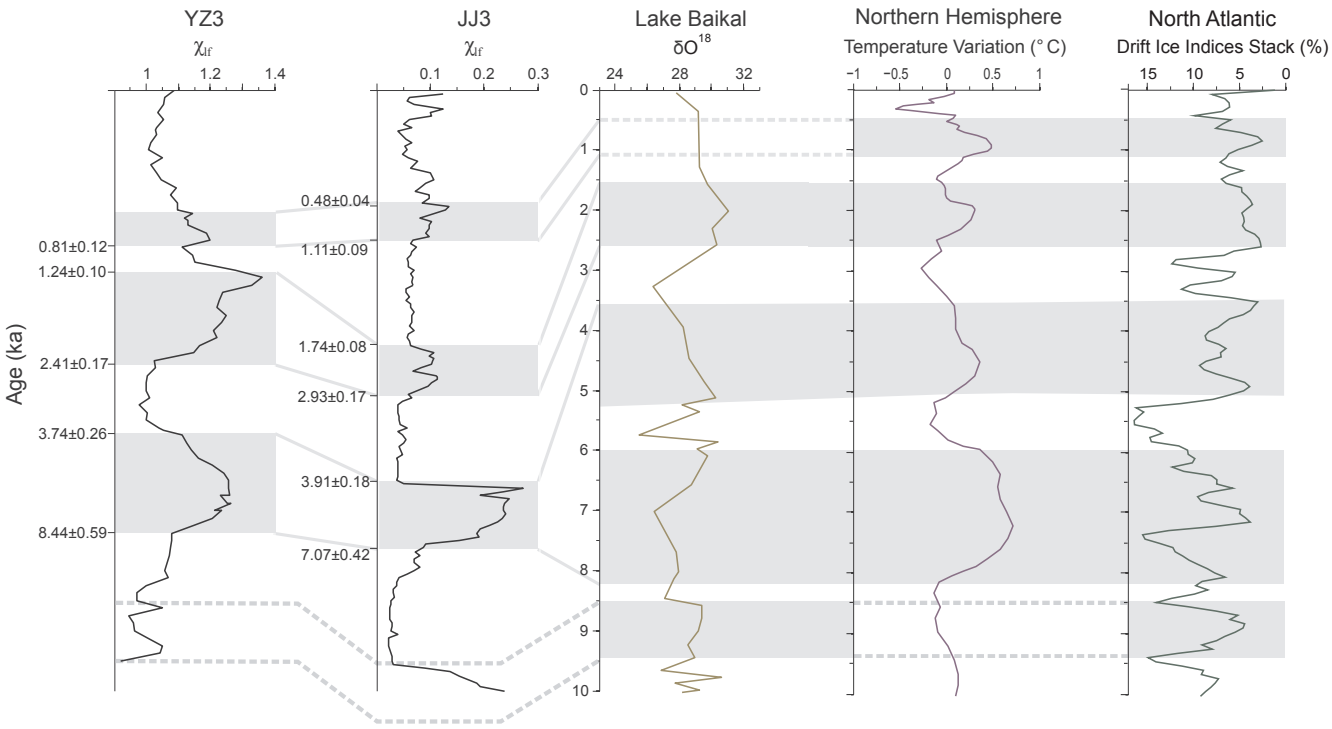

Fig. 7. Regional and global correlations (from south to north): χ_{lf} – low frequency magnetic susceptibility ($10^{-6}\,m^3\,kg^{-1}$) for YZ3 section (this study); χ_{lf} ($10^{-6}\,m^3\,kg^{-1}$) for JJ3 section (this study); Lake Baikal δO^{18} profile linked to mass-balancing isotope measurements in per mil deviations from VSMOW (Vienna Standard Mean Ocean Water) (Mackay et al., 2011); temperature variations (°C) in the northern hemisphere (relative to mean temperature during 1960–1980) averaged from multiple published sources (McMichael, 2012); and Drift Ice Indices Stack from North Atlantic (Bond et al., 2001). See Fig. 1 for the locations. Grey horizontal bars indicate the warm-wet climatic intervals based on the record of this study.

et al. (2011) reviewed that the global cooling event between ~3.3 and ~2.5 ka coincided with a considerably low solar activity forcing.

In Fig. 7, warmer interval of ~2.4–1.2 ka and colder interval of ~1.2–0.81 ka in the studied area correlate well with the $\delta^{18}O$ values of the Lake Baikal (Mackay et al., 2011), temperature variations in the northern hemisphere (McMichael, 2012), and Drift Ice Indices Stack from the North Atlantic (Bond et al., 2001). This event (~1.2–1.0 ka) corresponds to the maxima in the $\delta^{14}C$ and ^{10}Be records, indicating a weakening in solar output at this interval (Mayewski et al., 2004). At low latitudes, ~1.2–1.0 ka usually shows dry conditions in tropical Africa and monsoonal Pakistan (Gasse, 2000; 2001). During ~1.2–1.0 ka, atmospheric CO_2 surged moderately and caused variations in solar output resulting in drought in Yucatan (Hodell et al., 1991, 2001). The other warmer interval of ~0.81–0.48 ka also corresponds to temperature variations in the northern hemisphere (McMichael, 2012) and Drift Ice Indices Stack from the North Atlantic (Bond et al., 2001). However, the resolution of the $\delta^{18}O$ data from the Holocene sediments of the Lake Baikal is not very high (Mackay et al., 2011), and does not allow to evaluate this interval in detail.

Our results demonstrate that changes in petromagnetic parameters of the loess-paleosol and sand-paleosol sequences in the studied area correlate closely with variations in climate documented separately, as explored by other proxies. Such correspondence demonstrates the global connections among the continental climate in Asia and central Eurasia, temperature variations in the northern hemisphere, and oceanic climate of the North Atlantic.

6. Conclusions

(1) Results of our study indicate that subsequent warm-humid phase occurred in the regions of the Guanzhong Basin on the Chinese Loess Plateau and the Mu Us Desert during ~8.4–3.7 ka, ~2.4–1.2 ka, and ~0.81–0.48 ka, evidenced by the development of paleosols as well as high values of petromagnetic parameters in all sections.
(2) The Holocene climatic optimum period, in the studied regions, occurred between ~8.4 and ~3.7 ka.
(3) The Holocene climate record of the studied regions is consistent with the reported climate records from the tree pollen analysis along the south-to-north eastern Chinese Loess Plateau at that time, suggesting that the same climatic variation occurred in eastern monsoonal China.
(4) Our results correspond to the record of climate changes on regional and/or global scales, implying that similar climatic pattern of changes occurred in different regions of the world during the Holocene and the Holocene climatic optimum possibly took place at the same time interval all over the northern hemisphere.

Acknowledgements

We thank J. Jiao for his help with laboratory measurement and Ji Ma for her help in the field. We are grateful to J. Nie for his thoughtful suggestions before the manuscript was submitted. This study was funded by the National Science Foundation of China [41772027, 41372037] for R.Z. and Natural Sciences and Engineering Research Council of Canada (NSERC) for V.A.K.

Data availability

We release the data presented here to the public domain at https://www.pangaea.de/.

Author contributions

T.A., V.A.K., and R.Z. wrote the manuscript and contributed equally into all stages of the manuscript preparation, field work and data analysis, they also conceived the study; L.P.K. measured in the lab and participated in the data analysis; L. Ya and L. Yu organized and participated in the field trip.

References

Alverson, K.D., Bradley, R.S., Pedersen, T.F., 2003. Paleoclimate, Global Change and the Future. Springer, New York.
An, Z.S., Xiao, J.L., 1990. Study on the eolian dust flux over the Loess Plateau – an example. Chin. Sci. Bull. 35, 1627–1631.
An, Z.S., Kukla, G., Porter, S.C., Xiao, J.L., 1991. Late quaternary dust flow on the Chinese Loess Plateau. Catena 18, 125–132.
An, Z.S., Porter, S.C., Kutzbach, J.E., Wu, X.H., Wang, S.M., Liu, X.D., Li, X.Q., Zhou, W.J., 2000. Asynchronous Holocene optimum of the East Asian monsoon. Quat. Sci. Rev. 19, 734–762.
An, C.B., Tang, L.Y., Barton, L., Chen, F.H., 2005. Climate change and cultural response around 4000 cal yr B.P. in the western part of Chinese Loess Plateau. Quat. Res. 63, 347–352.
Baker, P.A., Seltzer, G.O., Fritz, S.C., Dunbar, R.B., Grove, M.J., Tapia, P.M., Cross, S.L., Rowe, H.D., Broda, J.P., 2001. The History of South American tropical precipitation for the past 25,000 years. Science 291, 640–643.
Balsam, W., Ji, J.F., Chen, J., 2004. Climatic interpretation of the Luochuan and Lingtai loess sections, China, based on changing iron oxide mineralogy and magnetic susceptibility. Earth Planet. Sci. Lett. 223, 335–348.
Bianchi, G.G., McCave, I.N., 1999. Holocene periodicity in north Atlantic climate and deep-ocean flow south of Iceland. Nature 397, 515–517.
Bond, G., Showers, W., Cheseby, M., Lotti, R., Almasi, P., deMenocal, P., Priore, P., Cullen, H., Hajdas, I., Bonani, G., 1997. A pervasive millenial-scale cycle in North Atlantic Holocene and glacial climates. Science 278, 1257–1266.
Bond, G., Kromer, B., Beer, J., Muscheler, R., Evans, M.N., Showers, W., Hoffmann, S., Lotti-Bond, R., Hajdas, I., Bonani, G., 2001. Persistent solar influence on north Atlantic climate during the Holocene. Science 294, 2130–2136.
Butler, R.F., 1992. Paleomagnetism: Magnetic Domains to Geologic Terranes. Blackwell Scientific Publications, Boston, MA.
Cosford, J., Qing, H., Eglington, B., Mattey, D., Yuan, D., Zhang, M., Cheng, H., 2008. East Asian monsoon variability since the Mid-Holocene recorded in a high-resolution, absolute-dated aragonite speleothem from eastern China. Earth Planet. Sci. Lett. 275 (3), 296–307.
D'Arrigo, R., Jacoby, G., Pederson, N., Frank, D., Buckley, B., Nachin, B., Mijiddorj, R., Dugarjav, C., 2000. Mongolian tree-rings, temperature sensitivity and reconstructions of Northern Hemisphere temperature. The Holocene 10 (6), 669–672.
Deng, C., Zhu, R., Verosub, K.L., Singer, M.J., Yuan, B., 2000. Paleoclimatic significance of the temperature-dependent susceptibility of Holocene loess along a NW-SE transect in the Chinese loess plateau. Geophys. Res. Lett. 27 (22), 3715–3718.
Deng, C.L., Zhu, R.X., Jackson, M.J., Verosub, K.L., Singer, M.J., 2001. Variability of the temperature-dependent susceptibility of the Holocene eolian deposits in the Chinese loess plateau: a pedogenesis indicator. Phys. Chem. Earth Part A 26 (11–12), 873–878.
Ding, Z.L., Rutter, N.W., Liu, T., 1993. Pedostratigraphy of Chinese loess deposits and climatic cycles in the last 2.5 Ma. Catena 20, 73–91.
Ding, Z.L., Yu, Z.W., Rutter, N.W., Liu, T.S., 1994. Towards an orbital time scale for Chinese loess deposits. Quat. Sci. Rev. 13, 39–70.
Dunlop, D.J., 2002. Theory and application of the Day plot (Mrs/Ms vs Hcr/Hc) 1. Theoretical curves and test using titanomagnetite data. J. Geophys. Res. 107, 4–22.
Evans, M.E., Heller, F., 2003. Environmental Magnetism: Principles and Applications of Enviromagnetics. Elsevier Science, Academic Press.
Feng, Z.D., An, C.B., Wang, H.B., 2006. Holocene climatic and environmental changes in the arid and semi-arid areas of China: a review. The Holocene 16, 119–130.
Feng, Z.-D., Thompson, L.G., Mosley-Thompson, E., Yao, T.D., 1993. Time-space model of climatic change in China during the past 10,000 years. The Holocene 3, 174–180.
Gasse, F., 2000. Hydrological changes in the African tropics since the last glacial maximum. Quat. Sci. Rev. 19, 189–211.
Gasse, F., 2001. Hydrological changes in Africa. Science 292, 2259–2260.
Hanesch, M., Stanjek, H., Petersen, N., 2006. Thermomagnetic measurements of soil iron minerals: the role of organic carbon. Geophys. J. Int. 165 (1), 53–61.
Haug, G.H., Hughen, K.A., Sigman, D.M., Peterson, L.C., Röhl, U., 2001. Southward migration of the intertropical Convergence zone through the Holocene. Science 293, 1304–1308.
He, Y., Theakstone, W.H., Zhang, Z.L., Zhang, D., Yao, T.D., Chen, T., Shen, Y.P., Pang, H.X., 2004. Asynchronous Holocene climatic change across China. Quat. Res. 61, 52–61.
Heller, F., Liu, T.S., 1984. Magnetism of Chinese loess deposits. Geophys. J. R. Astron. Soc. 77, 125–141.
Herzschuh, U., 2006. Palaeo-moisture evolution in monsoonal central Asia during the last 50,000 years. Quat. Sci. Rev. 25, 163–178.
Hodell, D.A., Curtis, J.H., Jones, G.A., Higuera-Gundy, A., Brenner, M., Binford, M.W., Dorsey, K.T., 1991. Reconstruction of Caribbean climate change over the past 10,500 years. Nature 352, 790–793.
Hodell, D.A., Brenner, M., Curtis, J.H., Guilderson, T., 2001. Solar forcing of drought frequency in the Maya Lowlands. Science 292, 1367–1370.
Hu, C., Henderson, G.M., Huang, J., Xie, S., Sun, Y., Johnson, K.R., 2008. Quantification of Holocene Asian monsoon rainfall from spatially separated cave records. Earth Planet. Sci. Lett. 266 (3), 221–232.
Huang, C.C., Zhou, J., Pang, J., Han, Y., Hou, C., 2000. A regional aridity phase and its

possible cultural impact during the Holocene Megathermal in the Guanzhong Basin, China. The Holocene 10 (1), 135–142.
Jacoby, G., D'Arrigo, R., Davaajamts, T.S., 2000. Mongolian tree-rings and 20th century warming. Science 273, 771–773.
Jin, G.Y., Liu, T.S., 2002. Mid-Holocene climate change in North China, and the effect on cultural development. Chin. Sci. Bull. 47, 408–413.
King, J.W., Channell, J.E.T., 1991. Sedimentary magnetism, environmental magnetism, and magnetostratigraphy. Rev. Geophys. 358–370.
King, J.W., Banerjee, S.K., Marvin, J., Ozdemir, O., 1982. A comparison of different magnetic methods for determining the relative grain size of magnetite in natural materials: some results from lake sediments. Earth Planet. Sci. Lett. 59, 404–419.
Klimenko, V.V., Klimanov, V.A., Fedorov, M.V., 1996. The history of the mean temperature of the Northern Hemisphere over the last 11,000 years. Trans. Russ. Acad. Sci. 4, 626–629.
Kravchinsky, V.A., Langereis, C.G., Walker, S.D., Dlusskiy, K.G., White, D., 2013. Discovery of Holocene millennial climate cycles in the Asian continental interior: Has the sun been governing the continental climate? Global Planet. Change 110, 386–396.
Li, J.J., 1996. Climatic change in arid areas of China and monsoon fluctuations during the past 10k years. J. Arid Environ. 32, 1–7.
Li, X.Q., Zhou, J., Dodson, J., 2003. The vegetation characteristics of the 'Yuan' area at Yaoxian on the Loess Plateau in China over the last 12000 years. Rev. Palaeobot. Palynol. 124, 1–7.
Li, G., Xia, D., Jia, J., Zhao, S., Gao, F., Wang, Y., Lu, H., Chen, F., 2015. Magnetic properties derived from a loess section at the northern piedmont of Tianshan Mountains, Xinjiang, China, and their paleoenvironmental significance. Geophys. J. Int. 203 (2), 828–839.
Licht, A., Pullen, A., Kapp, P., Abell, J., Giesler, N., 2016. Eolian cannibalism: reworked loess and fluvial sediment as the main sources of the Chinese Loess Plateau. Geol. Soc. Am. Bull. 128 (5–6), 944–956.
Liu, T.S., 1985. Loess and Environment. Science Press, Beijing, pp. 481.
Liu, Q., Jackson, M.J., Banerjee, S.K., Maher, B.A., Deng, C., Pan, Y., Zhu, R., 2004. Mechanism of the magnetic susceptibility enhancements of the Chinese loess. J. Geophys. Res. Solid Earth 109 (B12).
Liu, F., Feng, Z., 2012. A dramatic climatic transition at ~4000 cal. yr BP and its cultural responses in Chinese cultural domains. The Holocene 22 (10), 1181–1197.
Lu, H.Y., VanHuissteden, K.O., An, Z.S., Nugteren, G., Vandenberghe, J., 1999. East Asia winter monsoon variations on a millennial time-scale before the last glacial– interglacial cycle. J. Quat. Sci. 14, 101–110.
Lu, H.Y., VanHuissteden, K.O., Zhou, J., Vandenberghe, J., Liu, X.D., An, Z.S., 2000. Variability of East Asian winter monsoon in Quaternary climatic extremes in North China. Quat. Res. 54, 321–327.
Lu, H.Y., Yi, S.W., Liu, Z.Y., Mason, J.A., Jiang, D.B., Cheng, J., Stevens, T., Xu, Z.W., Zhang, E.L., Jin, L.Y., Zhang, Z.H., Guo, Z.T., Wang, Y., Otto-Bliesner, B., 2013. Variation of East Asian monsoon precipitation during the past 21 ky and potential CO_2 forcing. Geology 41 (9), 1023–1026.
Ma, J., Yue, L., Yang, L., Sun, L., Xu, Y., 2011. Southeastern margin of the Mu Us Desert Holocene sectional OSL's and paleoclimatic significance (in Chinese). Quaternary Sciences 31 (1), 120–129.
Mackay, A.W., Swann, G.E.A., Brewer, T., Leng, M.J., Morley, D.W., Piotrowska, N., Rioual, P., White, D., 2011. A reassessment of late glacial-Holocene diatom oxygen isotope records from Lake Baikal using a mass balance approach. J. Quat. Sci. 26 (6), 627–634.
Maher, B.A., 1988. Magnetic properties of some synthetic submicron magnetite. Geophys. J. 94, 83–96.
Maher, B.A., MengYu, H., Roberts, H.M., Wintle, A.G., 2003. Holocene loess accumulation and soil development at the western edge of the Chinese Loess Plateau: implications for magnetic proxies of palaeorainfall. Quat. Sci. Rev. 22 (5–7), 445–451.
Maher, B.A., 2011. The magnetic properties of Quaternary aeolian dust and sediments, and their palaeoclimatic significance. Aeolian Res. 3, 87–144.
Maher, B.A., Thompson, R., 1995. Paleorainfall reconstruction from pedogenic magnetic susceptibility variations in the Chinese loess and paleosols. Quat. Res. 44, 383–391.
Mayewski, P.A., Rohling, E.E., Stager, J.C., Karlén, W., Maasch, K.A., Meeker, L.D., Meyerson, E.A., Gasse, F., Kreveld, S.V., Holmgren, K., Lee-Thorp, J., Rosqvist, G., Rack, F., Staubwasser, M., Schneider, R.R., Steig, E.J., 2004. Holocene climate variability. Quat. Res. 62, 243–255.
McDermott, F., Mattey, D.P., Hawkesworth, C., 2001. Centennial-scale Holocene climate variability revealed by a highresolution speleothem 5180 record from SW Ireland. Science 294, 1328–1331.
McMichael, A.J., 2012. Insights from past millennia into climatic impacts on human health and survival. Proc. Natl. Acad. Sci. 109 (13), 4730–4737.
Meeker, L.D., Mayewski, P.A., 2002. A 1400-year high-resolution record of atmospheric circulation over the North Atlantic and Asia. Holocene 12, 257–266.
Mischke, S., Lai, Z., Long, H., Tian, F., 2016. Holocene climate and landscape change in the northeastern Tibetan Plateau foreland inferred from the Zhuyeze Lake record. The Holocene 26 (4), 643–654.
Mu, Y., Qin, X., Zhang, L., Xu, B., 2016. Holocene climate change evidence from high-resolution loess/paleosol records and the linkage to fire–climate change–human activities in the Horqin dunefield in northern China. J. Asian Earth Sci. 121, 1–8.
Nasrazadani, S., Raman, A., 1993. The application of infrared spectroscopy to the study of rust systems—II. Study of cation deficiency in magnetite (Fe_3O_4) produced during its transformation to maghemite (γ-Fe_2O_3) and hematite (α-Fe_2O_3). Corros. Sci. 34 (8), 1355–1365.
Nie, J., Stevens, T., Rittner, M., Stockli, D., Garzanti, E., Limonta, M., Bird, A., Andò, S., Vermeesch, P., Saylor, J., Lu, H., 2015. Loess plateau storage of northeastern Tibetan plateau-derived Yellow River sediment. Nat. Commun. 6, 8511.
Porter, S.C., 2001. Chinese loess record of monsoon climate during the last glacial–interglacial cycle. Earth Sci. Rev. 54 (1–3), 115–128.
Pye, K., Zhou, L.P., 1989. Late Pleistocene and Holocene aeolian dust deposition in North China and the Northwest Pacific Ocean. Palaeogeogr., Palaeoclimatol., Palaeoecol. 73, 11–23.
Rea, D.K., 1994. The paleoclimatic record provided by eolian deposition in the deep sea: the geologic history of wind. Rev. Geophys. 32, 159–195.
Robinson, S.G., 1986. The late Pleistocene paleoclimatic record of North Atlantic deep-sea sediments revealed by mineral-magnetic measurements. Phys. Earth Planet. Inter. 42, 22–47.
Rutter, N.W., 1992. Chinese loess and global change. Quat. Sci. Rev. 11, 275–281.
Shen, J., 2013. Spatiotemporal variations of Chinese lakes and their driving mechanisms since the Last Glacial Maximum: a review and synthesis of lacustrine sediment archives. Chin. Sci. Bull. 58 (1), 17–31.
Shen, C.M., Liu, K.-B., Tang, L.Y., Overpeck, J.T., 2006. Quantitative relationships between modern pollen rain and climate in the Tibetan Plateau. Rev. Palaeobot. Palynol. 140, 61–77.
Shi, Y.F., Kong, Z.C., Wang, S.M., 1992. Climatic variations and the major events in the Holocene Megathermal in China (in Chinese). Science in China 12, 300–308.
Steig, E.J., 1999. Mid-Holocene climate change. Science 286, 1485–1487.
Sun, J.M., 2000. Origin of eolian sand mobilization during the past 2300 years in the Mu Us Desert, China. Quat. Res. 53, 73–88.
Sun, J.M., Ding, Z.L., Liu, T.S., Rokosh, D., Rutter, N.W., 1999. 580,000-year environmental reconstruction from aeolian deposits at the Mu Us desert margin, China. Quat. Sci. Rev. 18, 1351–1364.
Sun, J.M., Li, S.H., Han, P., Chen, Y., 2006. Holocene environmental changes in the central Inner Mongolia, based on single-aliquot-quartz optical dating and multi-proxy study of dune sands. Palaeogeogr., Palaeoclimatol., Palaeoecol. 233, 51–62.
Sun, Q.L., Wang, S.M., Zhou, J., Shen, J., Cheng, P., Xie, X.P., Wu, F., 2009. Lake surface fluctuations since the late glaciation at Lake Daihai, North-central China: a direct indicator of hydrological process responses to East Asian monsoon climate. Quat. Int. 194, 45–54.
Tarasov, P., Jin, G.Y., Wagner, M., 2006. Mid-Holocene environmental and human dynamics in Northeastern China reconstructed from pollen and archaeological data. Palaeogeogr., Palaeoclimatol., Palaeoecol. 241, 284–300.
Thompson, R., Oldfield, F., 1986. Environmental Magnetism. Allen and Unwin, London.
Thompson, L.G., Mosley-Thompson, E., Davis, M.E., Bolzan, J.F., Dai, J., Yao, T., Gundestrup, N., Wu, X., Klein, Z., Xie, Z., 1989. Holocene-Late Pleistocene climatic ice core records from Qinghai-Tibetan Plateau. Science 246, 474–477.
Vandenberghe, J., An, Z.S., Nugteren, G., Lu, H.Y., VanHuissteden, K., 1997. New absolute time scale for the Quaternary climate in the Chinese loess region by grain-size analysis. Geology 25, 35–38.
Wang, H., Chen, J., Zhang, X., Chen, F., 2014. Palaeosol development in the Chinese Loess Plateau as an indicator of the strength of the East Asian summer monsoon: evidence for a mid-Holocene maximum. Quat. Int. 334, 155–164.
Wanner, H., Solomina, O., Grosjean, M., Ritz, S.P., Jetel, M., 2011. Structure and origin of Holocene cold events. Quat. Sci. Rev. 30 (21), 3109–3123.
Wen, R.L., Xiao, J.L., Chang, Z.G., Zhai, D.Y., Xu, Q.H., Li, Y.C., Itoh, S., 2010. Holocene precipitation and temperature variations in the East Asian monsoonal margin from pollen data from Hulun Lake in northeastern Inner Mongolia, China. Boreas 39, 262–272.
Wurster, C.M., Patterson, W.P., 2001. Late Holocene climate change for the eastern interior United States. Evidence from highresolution 6180 value of marital otoliths. Palaeogeogr., Palaeoclimatol., Palaeoecol. 170, 81–100.
Xiao, J.L., Xu, Q.H., Nakamura, T., Yang, X.L., Liang, W.D., Inouchi, Y., 2004. Holocene vegetation variation in the Daihai Lake region of north-central China: a direct indication of the Asian monsoon climatic history. Quat. Sci. Rev. 23, 1669–1679.
Yang, S.L., Ding, Z.L., 2004. Comparison of particle size characteristics of the Tertiary 'red clay'and Pleistocene loess in the Chinese Loess Plateau: implications for origin and sources of the 'red clay'. Sedimentology 51 (1), 77–93.
Yang, X.P., Scuderi, L., Paillou, P., Liu, Z.T., Li, H.W., Ren, X.Z., 2011. Quaternary environmental changes in the drylands of China-a critical review. Quat. Sci. Rev. 30, 3219–3233.
Yu, L., Oldfield, F., 1989. A multivariate mixing model for identifying sediment source from magnetic measurements. Quat. Res. 32, 168–181.
Zhao, C., Yu, Z., Zhao, Y., Ito, E., Kodama, K.P., Chen, F., 2010. Holocene millennial-scale climate variations documented by multiple lake-level proxies in sediment cores from Hurleg Lake, Northwest China. J. Paleolimnol. 44 (4), 995–1008.
Zhao, H., Chen, F.H., Li, S.H., Wintle, A.G., Fan, Y.X., Xia, D.S., 2007. A record of Holocene climate change in the Guanzhong Basin, China, based on optical dating of a loess-palaeosol sequence. The Holocene 17 (7), 1015–1022.
Zhao, Y., Yu, Z., 2012. Vegetation response to Holocene climate change in East Asian monsoon-margin region. Earth Sci. Rev. 113 (1), 1–10.
Zhang, Y., Kong, Z., Zhang, Q.B., Yang, Z., 2015. Holocene climate events inferred from modern and fossil pollen records in Butuo Lake, Eastern Qinghai-Tibetan Plateau. Climatic Change 133 (2), 223–235.
Zhou, W.J., An, Z.S., 1994. Stratigraphic divisions of the Holocene loess in China. Radiocarbon 36, 37–45.
Zhou, W.J., Yu, S.-Y., Georges, B., Kukla, G.J., Jull, A.J.T., Xian, F., Xiao, J.Y., Colman, S.M., Yu, H.G., Liu, Z., Kong, X.H., 2010. Postglacial changes in the Asian summer monsoon system: a pollen record from the eastern margin of the Tibetan Plateau. Boreas 39, 528–539.
Zhu, Z.D., Liu, S., He, R.Z., 1982. Deserts evolution in the historic time, physical geography of China. Hist. Geogr. 6, 249–253.

Supplementary figures for the manuscript

Holocene climatic evolution at the Chinese Loess Plateau: testing sensitivity to the global warming-cooling events

Taslima Anwar[a,b], Vadim A. Kravchinsky[b,a,*], Rui Zhang[a,b,c,*], Lioudmila P. Koukhar[b], Lirong Yang[a], Leping Yue[a,c]

[a] State Key Laboratory of Continental Dynamics, Department of Geology, Northwest University, Xi'an 710069, China

[b] Department of Physics, University of Alberta, Edmonton, Alberta, T6G 2E1, Canada

[c] State Key Laboratory of Loess and Quaternary Geology, Institute of Earth Environment, Chinese Academy of Sciences, Xi'an 710075, China

[*] *Correspondence to:* Vadim A. Kravchinsky (vadim@ualberta.ca) and Rui Zhang (zhangrui2000@qq.com)

Journal of Asian Earth Sciences

2018

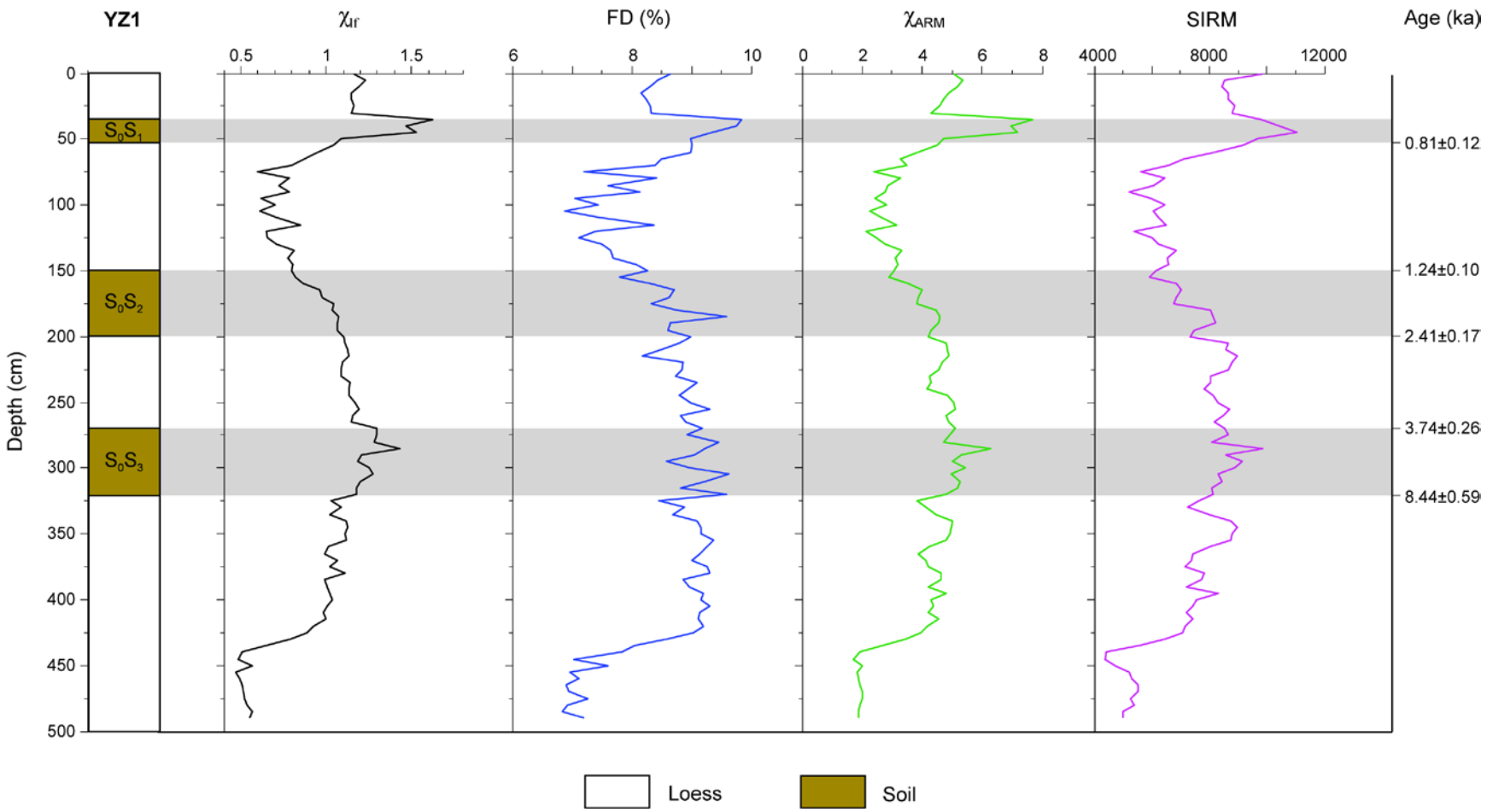

Supplementary Figure 1. Stratigraphy and magnetic concentration parameters of the YZ1 section. χ_{lf} – low frequency magnetic susceptibility (10^{-6} m^3 kg^{-1}); FD (%) – frequency dependence parameter; χ_{ARM} – anhysteric remanent magnetization (10^{-6} m^3 kg^{-1}); and SIRM– saturation isothermal remanent magnetization (10^{-6} Am^2 kg^{-1}). Horizontal grey bars denote soil horizons, interpreted as relatively warm-wet intervals.

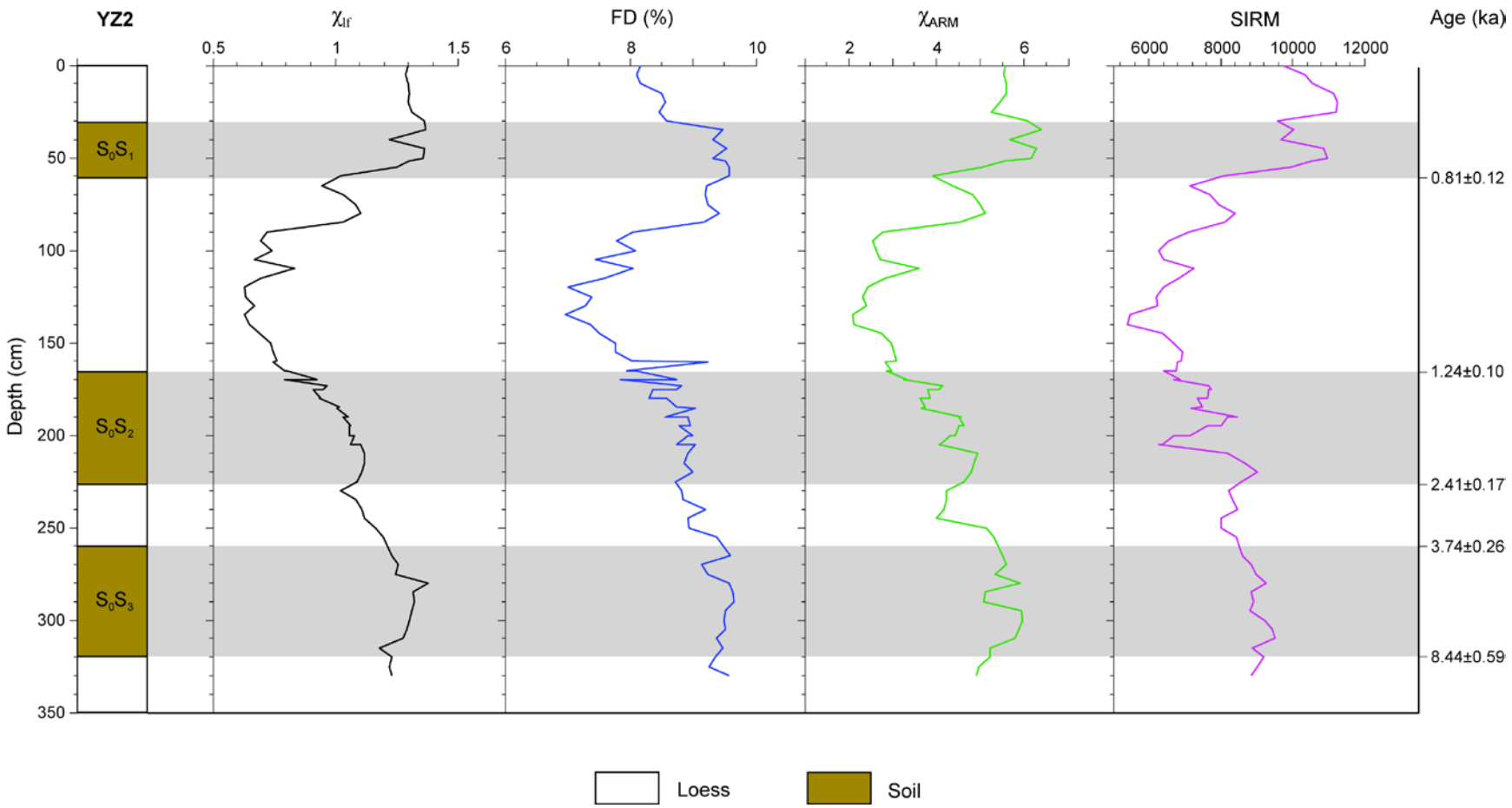

Supplementary Figure 2. Stratigraphy and magnetic concentration parameters of the YZ2 section. Same abbreviations as in Supp. Fig. 1.

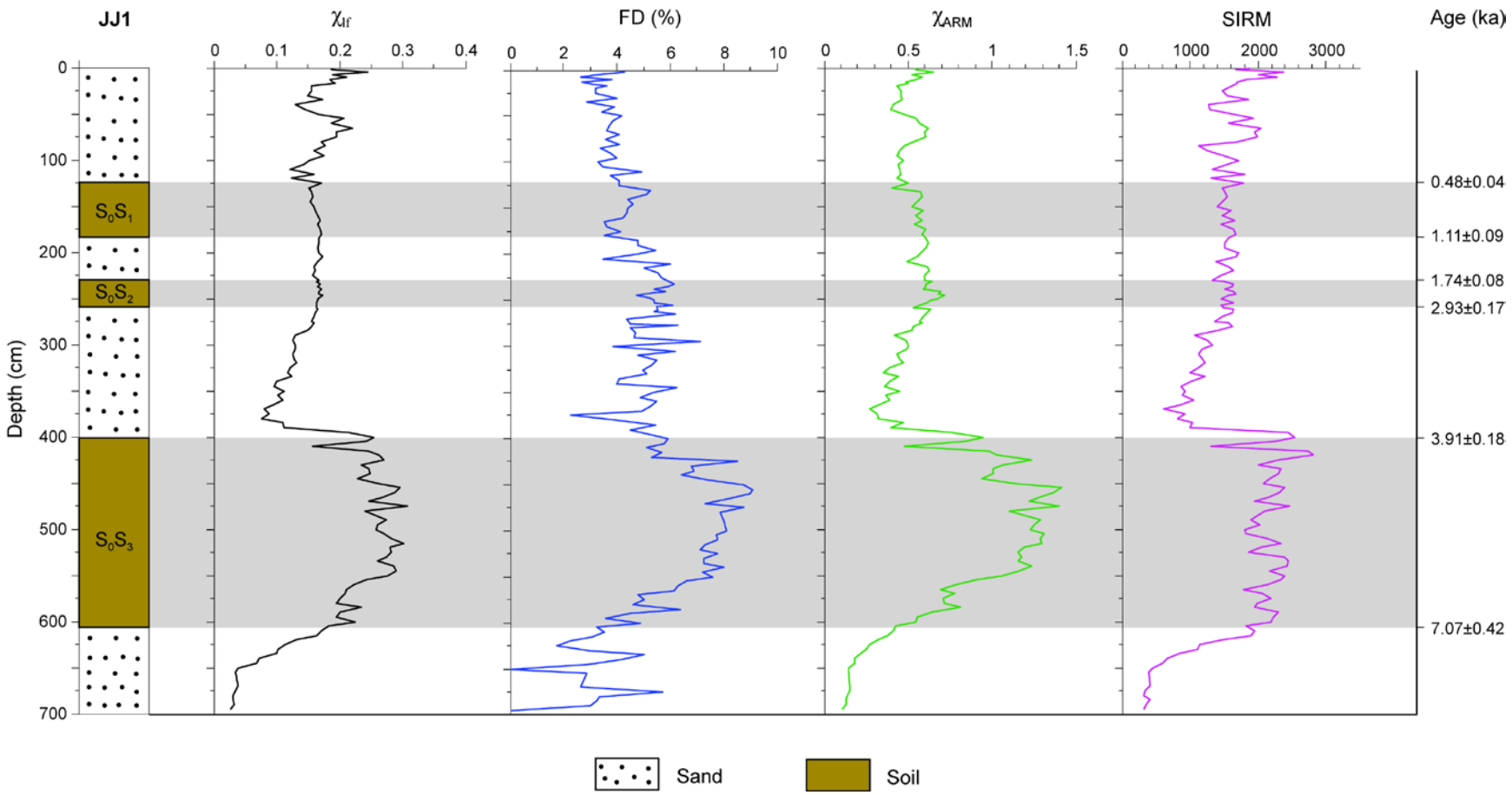

Supplementary Figure 3. Stratigraphy and magnetic concentration parameters of the JJ1 section. Same abbreviations as in Supp. Fig. 1.

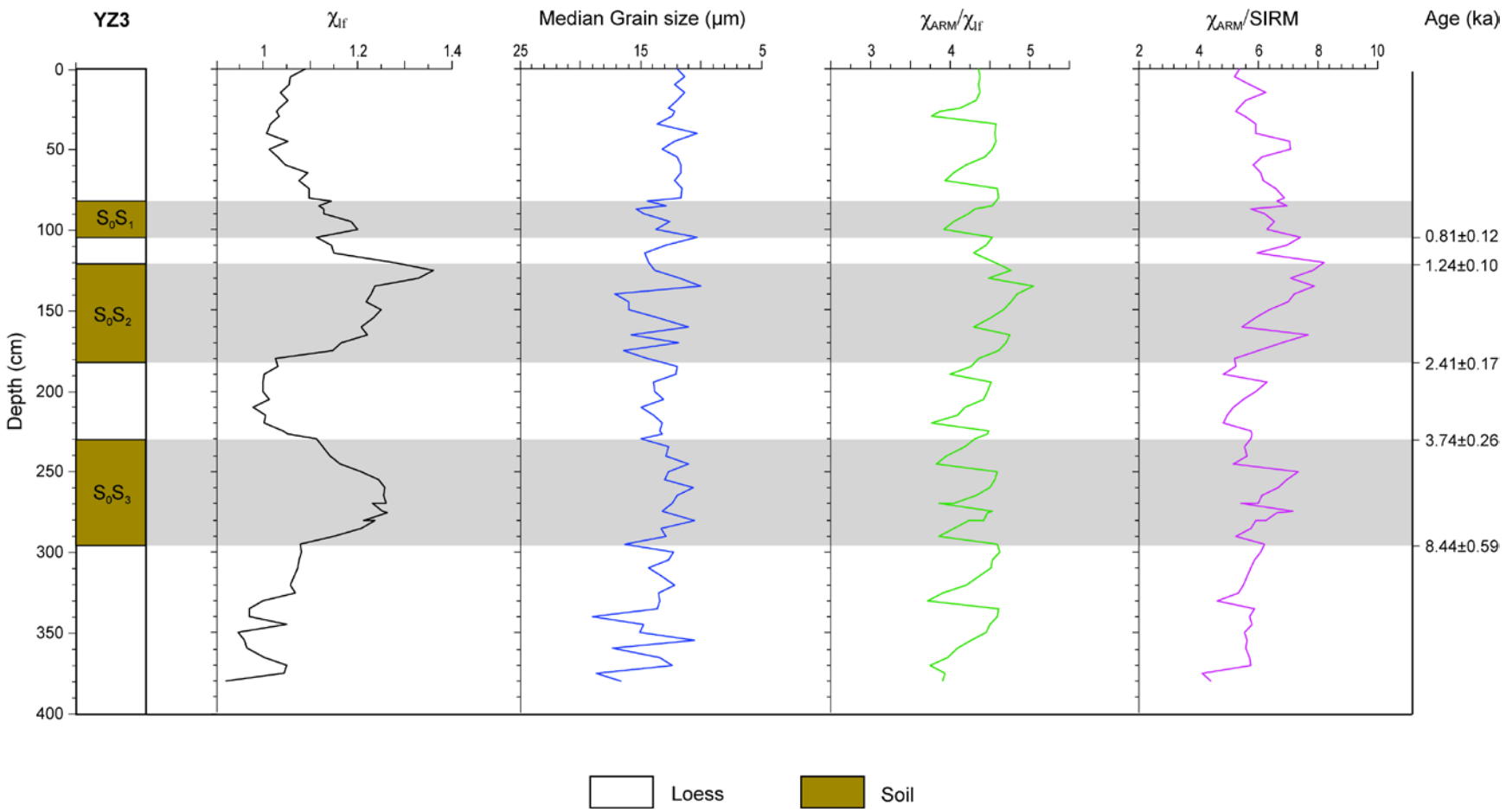

Supplementary Figure 4. Stratigraphy and analytic data for the YZ3 section. χ_{lf} – low frequency magnetic susceptibility (10^{-6} m^3 kg^{-1}); MD – median sedimentary grain size (μm); χ_{ARM}/χ_{lf} – magnetic grain size parameter (unitless); and $\chi_{ARM}/SIRM$ – magnetic grain size parameter (10^{-4} mA^{-1}). Horizontal grey bars denote soil horizons, interpreted as relatively warm-wet intervals.

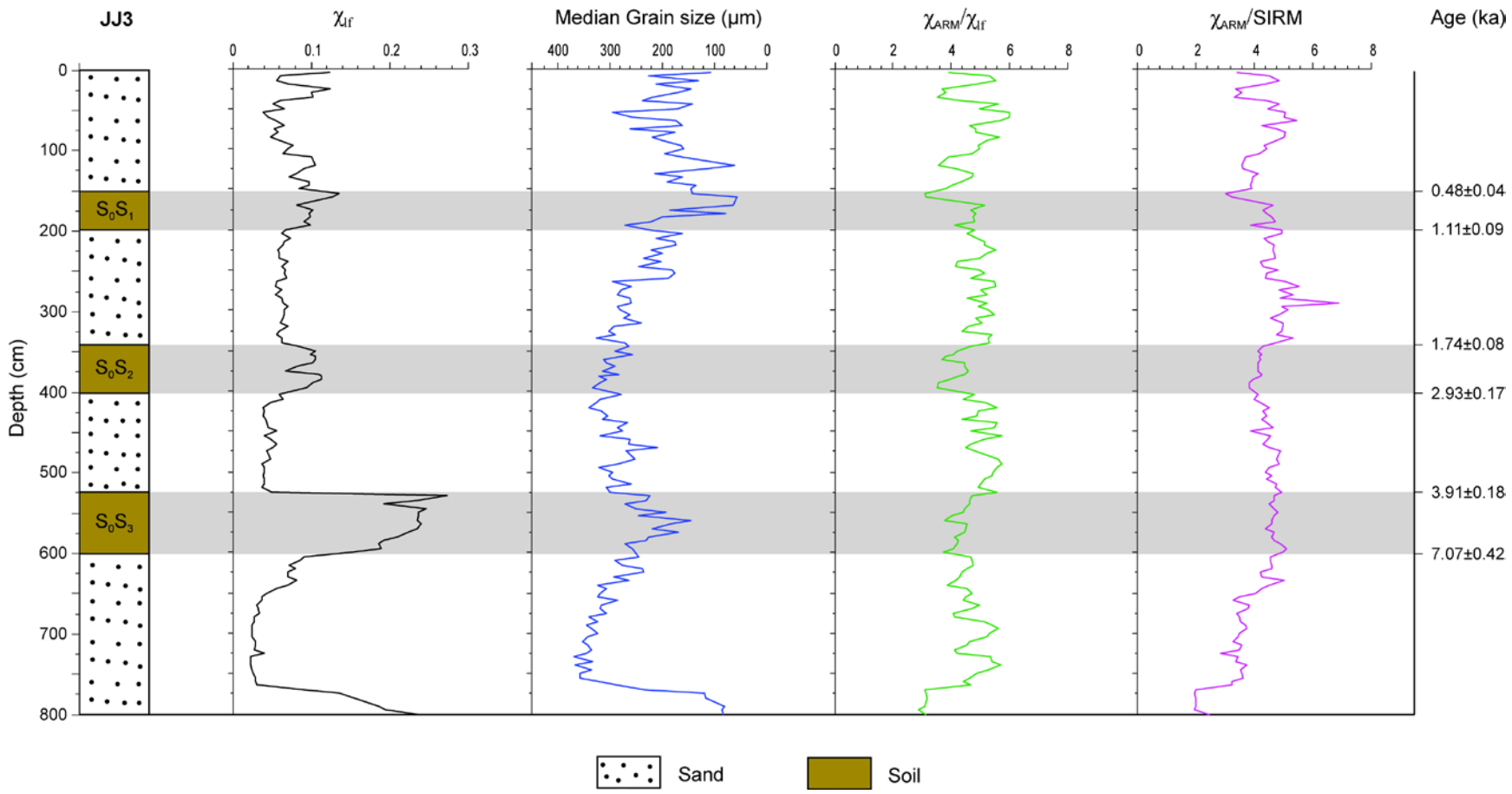

Supplementary Figure 5. Stratigraphy and analytic data for the JJ3 section. Same abbreviations as in Supp. Fig. 4.